J Polym Res (2014) 21:481
DOI 10.1007/s10965-014-0481-9

ORIGINAL PAPER

Shape memory effect for recovering surface damages on polymer substrates

Nuria García-Huete · José Manuel Laza · José María Cuevas · Beatriz Gonzalo · José Luis Vilas · Luis Manuel León

Received: 20 February 2014 / Accepted: 9 May 2014 / Published online: 16 May 2014

Abstract Self-repair properties based on shape-memory features of covalently crosslinked semi-crystalline polyalkenamers were demonstrated by thermal-activated recovery of performed surface marks (indented holes and scratches). Shape memory polymers were prepared by mixing a commercial polycyclooctene (PCO) with different percentages of peroxide, and then these mixtures were processed by compression moulding to obtain crosslinked sheets. With the aid of a hardness test pencil, holes and scratches in the surface of the materials were realized with different known forces (5, 10 and 15 N). The disappearance of surface defects was evaluated using both optical and contact surface profilometry, as well as optical microscopy under heating processes. This technique allowed evaluating shape recovery ratios of edgewise holes in PCO samples. In parallel, the analysis of maximum depth of indentations with temperature for edgewise samples by optical microscopy allows evaluating shape recovery. As a complementary tool for analysing thermal shape-recovery and surface resistance to indentation, thermal properties and hardness were investigated by DSC and Shore durometer test, respectively.

Keywords Smart materials · Shape memory polymer · Semi-crystalline polymer · Self-repair · Indentation

N. García-Huete · J. L. Vilas
Basque Center for Materials, Applications and Nanostructures (BCMaterials), Parque Tecnológico de Bizkaia, Ed. 500, Derio 48160, Spain

J. M. Laza (✉) · L. M. León
Departamento de Química Física, Facultad de Ciencia y Tecnología, Universidad del País Vasco/EHU, Apdo.644, Bilbao 48080, Spain
e-mail: josemanuel.laza@ehu.es

J. M. Cuevas · B. Gonzalo
Gaiker Technology Centre, Parque Tecnológico de Bizkaia, Ed. 202, Zamudio 48170, Spain

Introduction

Most of the polymeric systems are susceptible to damage from environmental stresses, which can cause loss in its mechanical, physical and aesthetic properties, so interest in developing and characterizing self-healing materials has grown considerably due to broad applicability in innumerable industrial sectors. Self-healing in materials, where damage is detected and repaired in situ [1, 2], is the result of a new and innovative approach to tailor the structure/property relations in materials to extend their lifetime and their reliability in use. Therefore, providing self-healing properties to these polymeric materials is enormously attractive from the industrial viewpoint. In recent years, different types of developed systems demonstrate the ability to heal, which are mainly based on microcapsule dispersions [3–5], particle segregation [6, 7], microvascular networks [8–10], or gels [11–14], among others, where shape memory polymers can play an outstanding role in the field of self-repairing features [15].

Shape memory polymers (SMPs) are those capable of recovering their original shape after having been deformed into a different one (temporary shape), i.e. they 'remember' the shape they were given when processed (permanent shape) on the basis of entropy changes with the ability of coming back to it several times (deformation cycles) from potential different temporary shapes. This ability is supported on appropriate molecular structures [16–19], where several SMPs based on different structures and functionalities exist [20, 21].

The shape memory effect can be induced under appropriate stimulus such as temperature [20–25]. Shape memory effect in these thermo-responsive SMPs normally consists of heating up the sample, deforming, and cooling the sample. The permanent shape is now stored while the sample shows the temporary shape. Heating up the shape memory polymer above a transition temperature T_{trans} induces the shape memory effect, and, as a consequence, the recovery of the stored permanent shape can be observed.

Furthermore, the deformation force may also be applied to a non-heated SMP, i.e. draw the sample at a low temperature. In this case, the permanent shape was recovered at an elevated temperature under a stress free condition [26]. Mather et al. [27] called it 'reversible plasticity shape memory effect (RP-SME)' and the deformation step is usually called 'cold drawing programming process' because it consists in working at temperatures below T_{trans} [20, 28], that is, deforming the SMP at glassy or crystalline state. This procedure has different benefits, such as lower recovery temperatures and largely enhanced recovery stress [29].

This effect (RP-SME) can be used to repair surfaces. The surface of the plastic-made objects may be damaged during its lifetime. These damages are mainly plastic deformations, which can be recovered according to RP-SME mechanism, although just in case of non-permanent damages such as surface scratches or indents. If permanent damages such cracking occur, heating would reduce crack width but not heal it [30] since surface scratches are material deformations related with entropy changes, whereas cracking implies a microscopical material separation. Thus, shape memory polymers can be used to partially repair structural damage [31].

In this scenario, the present study describes the potential thermally activated self-repair features of developed polyalkenamer based shape memory materials faced to thermomechanical and shape memory properties, as a function of the degree of selective crosslinking of the semi-crystalline network. Therefore, these polymers can recover its original shape upon heating above its melting temperature (Tm), due to its autonomous conformational entropy driven shape recovery mechanism, which is demonstrated by different techniques, such as surface profilometry, and confocal and optical microscopy.

Experimental

Materials

Vestenamer® 8012 (Evonik) in pellet form, which is a 99.5 % purity low broad molecular weight polyoctenamer (PCO) consisting of linear and cyclic macromolecules with 80 % of its double bonds arranged in a crystallizable *trans* configuration, was used as received without any previous purification step. The crosslinking agent used was dicumyl peroxide (DCP) from Aldrich, which is a 98.0 % purity solid crystalline monofunctional peroxide.

Preparation of samples

Shape memory systems were prepared as previously described [32], i.e. polycyclooctene (PCO) Vestenamer® 8012 and 1, 2 and 3 wt% dicumyl peroxide (DCP) were blended using a Haake Rheomix 600 mixing chamber at 70ºC and subsequently crosslinked at 180ºC for 20 min by compression moulding under a pressure of 925 bar in a 2 mm thickness flat mould. Two Teflon sheets were placed on both sides of the mould to reduce the surface roughness of the PCO-DCP specimens obtained. After curing, the obtained 50 mm × 50 mm × 2 mm specimens were cooled to room temperature in the mould under constant pressure. In order to provide an identical thermal history, the neat PCO (0 wt% of peroxide) was also processed under the same described conditions. Table 1 summarizes all the developed PCO samples.

Experimental methods

Thermal Properties

Thermal properties of neat PCO and crosslinked PCO samples were measured by Differential Scanning Calorimetry (DSC 822e from Mettler Toledo) to identify thermal actuation temperatures. Samples in aluminium pans were characterized under constant nitrogen flow (50 ml·min^{-1}). First, samples were heated from −100 to 150ºC at a rate of 10ºC·min^{-1}, followed by a cooling scan from 150 to −100ºC at a rate of −10ºC·min^{-1}. Subsequently, a second heating scan to 150ºC was conducted at the same heating rate. In all cases, samples around 10–12 mg were used.

The DSC analysis indicated that the peroxide concentration, and the associated crosslinking density, has an impact on the crystallinity of the materials. Crystallinity values, calculated as it was explained in a previous work from enthalpy of 100 % crystalline PCO [32], were also shown in Table 1. It should be noted that both Tm as crystallinity values reported in reference 33 are slightly different from those shown in Table 1 (in this work, Tm values are slightly higher while the crystallinity is slightly lower). These differences are due to two facts: 1) the PCO was used as received without purification and therefore small differences both in composition as in molecular weight are possible between batches, and 2) the DCP employed in this work was an Aldrich product (98.0 % purity) whereas in previous works was used a AKZO Nobel Polymer Chemicals DCP (99.0 % purity).

Table 1 Thermal properties of the PCO-DCP samples studied

Sample	DCP wt%	Tg (ºC)	Tm (ºC)	Trec (ºC)	Crystallinity (%)
PCO-0	0	−76.3	57.0	80	26.4
PCO-1	1	−75.5	52.6	70	24.8
PCO-2	2	−73.6	42.0	60	22.2
PCO-3	3	−73.5	37.8	55	20.7

Shore D hardness

Shore test measures the resistance of plastics toward indentation. Thus, Shore D hardness of different PCO samples was measured by pressing a 30° cone indenter tip of 1.4 mm extension with a spring force of 44.48 N on the surface with a Shore D mechanical hardness tester, assembled on test stand BS 61 from BAREISS PRÜFGERÄTEBAU GMBH, and reading the scale after 15 s holding the presser foot in contact. Five measurements of hardness were performed and the median value was determined.

Self-repair behaviour

Shape memory properties of crosslinked PCO samples were evaluated using surface profilometry (Alpha-Step D-100 profilometer from KLA-Tencor), non-contact confocal optical 3D profilometer (PLμ NEOX microscope from SENSOFAR) and optical microscopy (NIKON SMZ-2 T optical microscope equipped with a CCTV camera, JenoptikC10Plus model). After measuring the surface roughness of the PCO specimens by optical-confocal profilometry test, holes were performed using a Hardness Test Pencil Model 318 from ERICHSEN by marking the surface of the samples with a known force (5, 10 and 15 N). Once the required spring tension is set, the Test Pencil was held upright and placed its point on the test surface to draw a hole. The length of contact time under load was very short (1–2 s) in order to minimise the effect of loading cycle time on final permanent deformation. Therefore, the deformation was applied to a non-heated samples and could be recovered at elevate temperature under stress free conditions [26] through the reversible shape memory plasticity effect described by Matter [27]. Subsequently, hole depths were measured using both surface and optical-confocal profilometry after marking and afterwards, after 24 h, using confocal microscopy.

The thermal-induced recovery process was observed using an optical microscope. The samples were put on a heating plate under the microscope until recovery process was finished and photos at different temperatures were taken. Finally, the PCO specimens were cooled down to room temperature previous to measure its profile using confocal microscopy.

In parallel, in order to evaluate the shape recovery ratios faced to temperature, the variation in the hole depths were measured following the recovery phase under heating process of perpendicular cuts of the performed marks on replicas by optical microscopy.

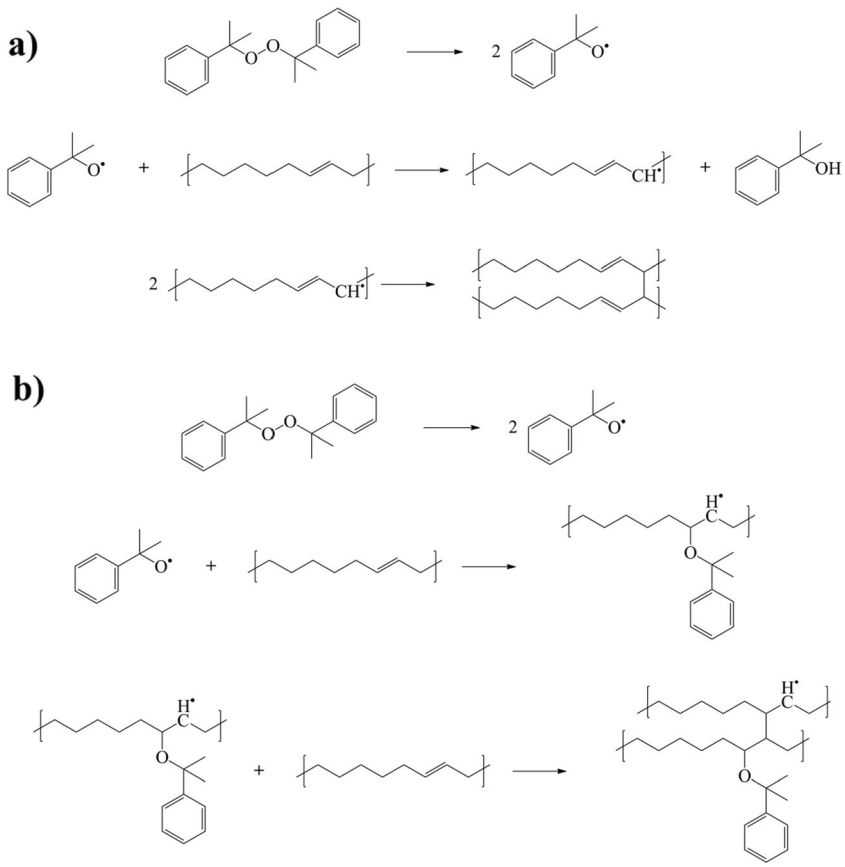

Scheme 1 Schematic representation of crosslinking reaction between PCO and DCP

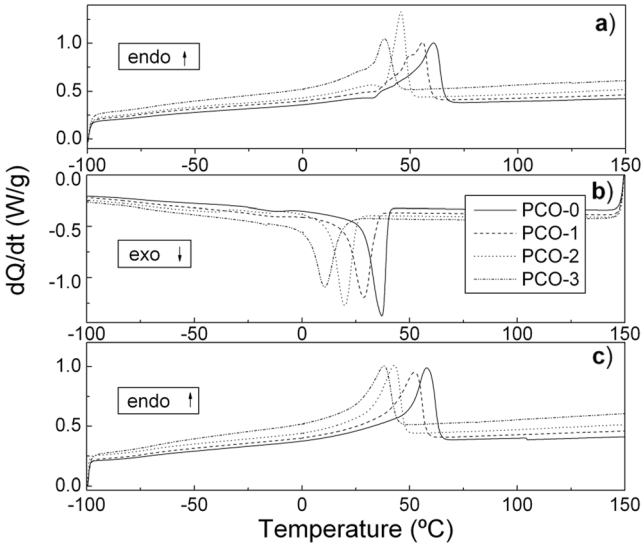

Fig. 1 DSC curves for all the PCO-DCP samples: **a** first heating, **b** cooling and **c** second heating

Moreover, to emphasize the potentiality of self-repairing capabilities, another test was effectuated by performing 30 mm line marks in PCO samples at a rate of approximately 10 mm·sec^{-1} with each force (5, 10 and 15 N) using the same Hardness Test Pencil. Measurements were made with the surface profilometer, again, before and after marking, 24 h later and after heating the sample in an oven during 10 min at approximately 20ºC above its melting temperature (Trec in Table 1) and cooling down.

Results and discussion

Crosslinking the macromolecular chains of the polymer using organic peroxides is a reported method to obtain shape memory polymers, as demonstrate described smart materials from polyethylene [33, 34], vinyl acetate [35] and polyvinyl chloride [20]. Moreover, Mather [36–38] and Lendlein [39] have synthesized crosslinked thermo-sensitive shape memory polymers using polycycloalkenes. In our group, magneto-active polymers [40], thermo-responsive polymers [32], shape memory composites [41], and triple-shape memory polymers [42] were obtained by balancing competitive crystallinity and elasticity via a monofunctional peroxide based crosslinking process.

In summary, the crosslinking process of the thermoplastic matrix promoted by dicumyl peroxide may occur via two main different reactions [43, 44] (Scheme 1). On the one hand, the free radicals from thermal decomposition of functional peroxide generate, by hydrogen abstraction, polymeric macroradicals able to react and recombine (Scheme 1a) in a crosslinked network. Besides, another process can occurs from combining the peroxide radical with the double bond of the polymer chain (Scheme 1b).

Table 2 Hole depth marks in the PCO-DCP samples

Sample	Shore D Hardness	Marking force (N)	Hole depth measured (μm)	
			Profilometry	Confocal microscopy
PCO-1	35.3	15	196	181
		10	79	86
		5	34	36
PCO-2	32.6	15	188	191
		10	130	133
		5	44	54
PCO-3	28.6	15	117	105
		10	106	100
		5	48	42

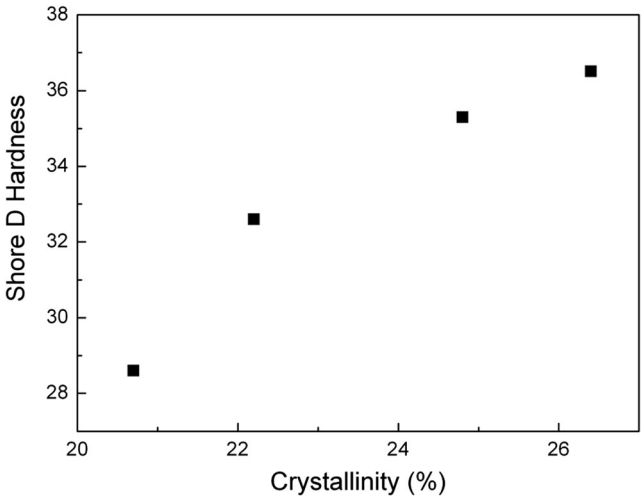

Fig. 2 Relationship between crystallinity and Shore D Hardness for PCO samples

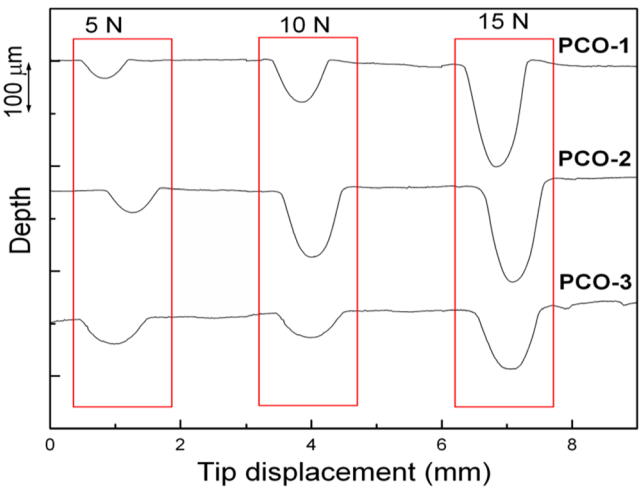

Fig. 3 Measured profiles of holes for all PCO samples

Thermal properties

Related to the thermal properties of the PCO-DCP measured by DSC, Fig. 1 shows the respective DSC curves, as well as Table 1 listed the corresponding melting temperatures. As can be observed in Fig. 1, the peaks corresponding to the melting and crystallization temperatures for the different PCO-DCP samples switched to lower temperatures as the DCP wt% increases. Increasing peroxide concentration, thus, promotes crosslinking density, and the degree of crystallinity decreases as result of the lower chain mobility from crosslinking knots, which are responsible for a lower diffusion and limited conformational order of the polymer chains.

Since slight differences in the DSC curves can be observed between consecutive heating cycles due to variations in the thermal history of the samples, the transition temperature of shape memory effect (T_{trans}) was defined from melting temperature measured in the second heating cycle (Tm in Table 1).

In conclusion, it is possible to tailor the melting temperature of the PCO-DCP crosslinked samples, and thus the transition temperature of shape memory (T_{trans}), simply by controlling the degree of crosslinking of the samples by the concentration of peroxide.

Self-repair behaviour

Hardness of semicrystalline polymers depends on numerous microestructural parameters related to crystallinity degree, conformational alternating lamellae regions and disordered

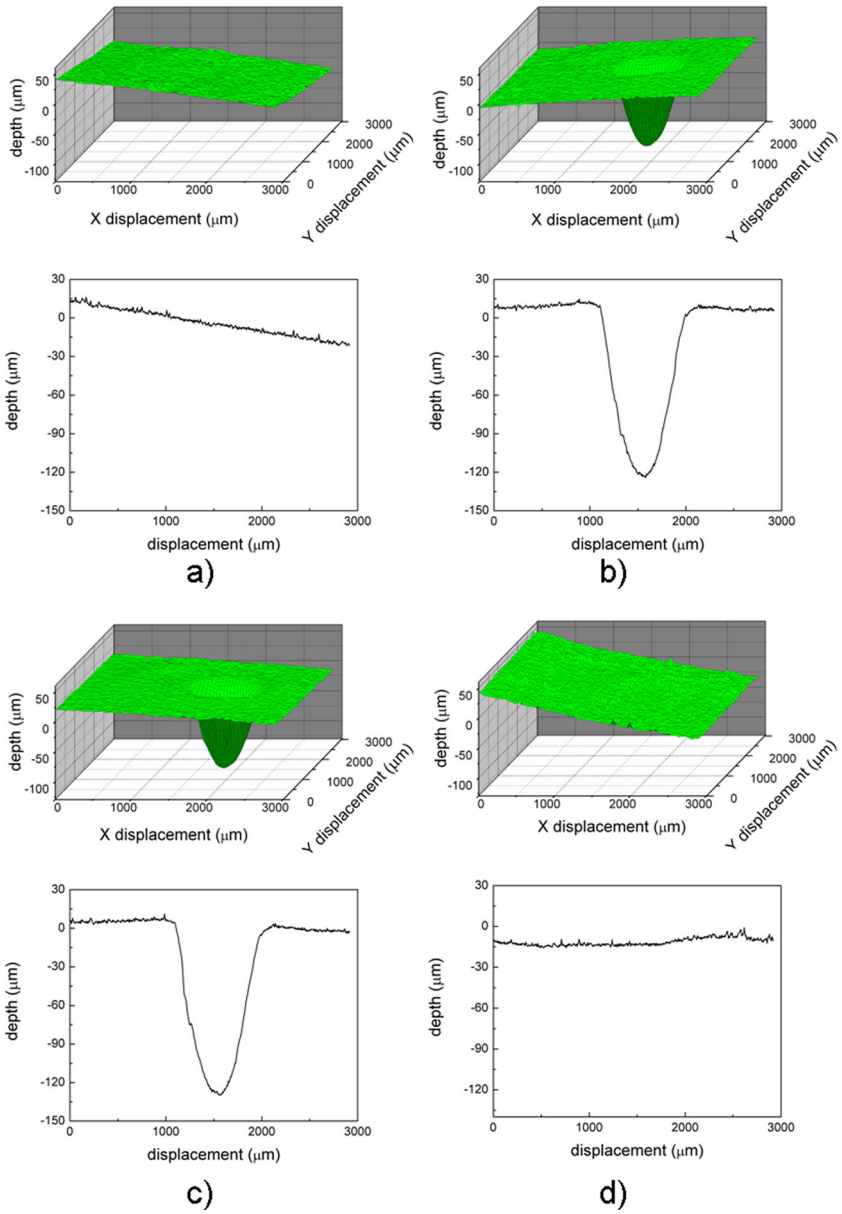

Fig. 4 Measured surfaces (*up*) and profiles (*down*) for 10 N hole in PCO-2 sample: (**a**) without hole, (**b**) hole, (**c**) measure 24 h later and (**d**) recovered

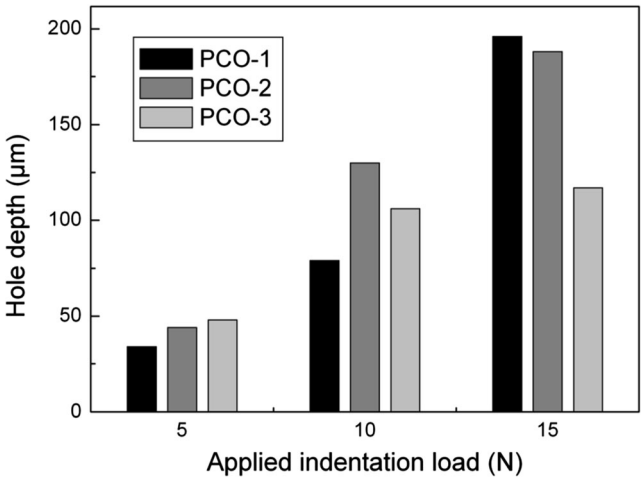

Fig. 5 Indentation depth vs. applied load for different crosslinked samples

layers, defects in the stereo regularity, chain entanglements and folds, and other conformational irregularities [45, 46]. However, hardness is often correlated to the yield stress, being a direct relationship between yield stress and degree of crystallinity, in agreement with data in Fig. 2 [47].

The measured depths in the centre of the holes from marking all samples with Test Pencil, evaluated by both profilometry techniques, are collected in Table 2, as well as corresponding Shore D hardness (for PCO-0 sample Shore D hardness is 36.5). Furthermore, the profiles obtained with the profilometry technique are illustrated in Fig. 3 for PCO-1, PCO-2 and PCO-3, respectively, whereas in Fig. 4 are shown both the measured surfaces and the corresponding profiles obtained with the confocal microscopy.

The depth values obtained by the two techniques (profilometry and confocal microscopy) are very similar following the same trend, which demonstrates that indentation depth increases with applied load for all cases (Fig. 5), and that both measurement techniques are appropriated for evaluating the subsequent self-repair behaviour.

Considering the hardness as a measurement of the resistance of the samples towards indentation, it could be expected lower indentation marks with higher hardness, as occurs for low indentation loads and related minor marking depths or deformations (Fig. 5). However, at the same time that applied load and subsequent depth increase, this trend reverses.

In semicrystalline polymers, the relationship between morphological characteristics and hardness is extremely complex and is dependent on many variables controlled by molecular weight, chain structure, degree of crystallinity, crystalline structure, thickness distribution of crystallites, interfacial interaction with non-crystalline region and structure of amorphous phase, among others [46].

Crosslinked PCO consists of separate and mechanically distinct 'hard' crystalline elements and 'soft' amorphous regions. Therefore, when indented, the material is compressed and a complex combination of effects influences the produced local deformation, being the prevalent mechanism dependent on the strain/stress field depth round the indent and on the morphology of the polymer [45]. Therefore, it is suspected that for low strains from low-moderate applied loads, probably prior to the yield point, deformation modes and strength of crystalline phase governs the observed performance. However, as the fraction of amorphous phase increases from lower crystallinity degree, when indentation involves yielding of crystalline regions and partial destruction of surface crystallites from higher strains, intrinsic flexibility and elastic storage properties of amorphous crosslinked chains prevails. Therefore, for high loads, when the applied stress is removed, the rubber-elastic behaviour of crosslinked molecules in the

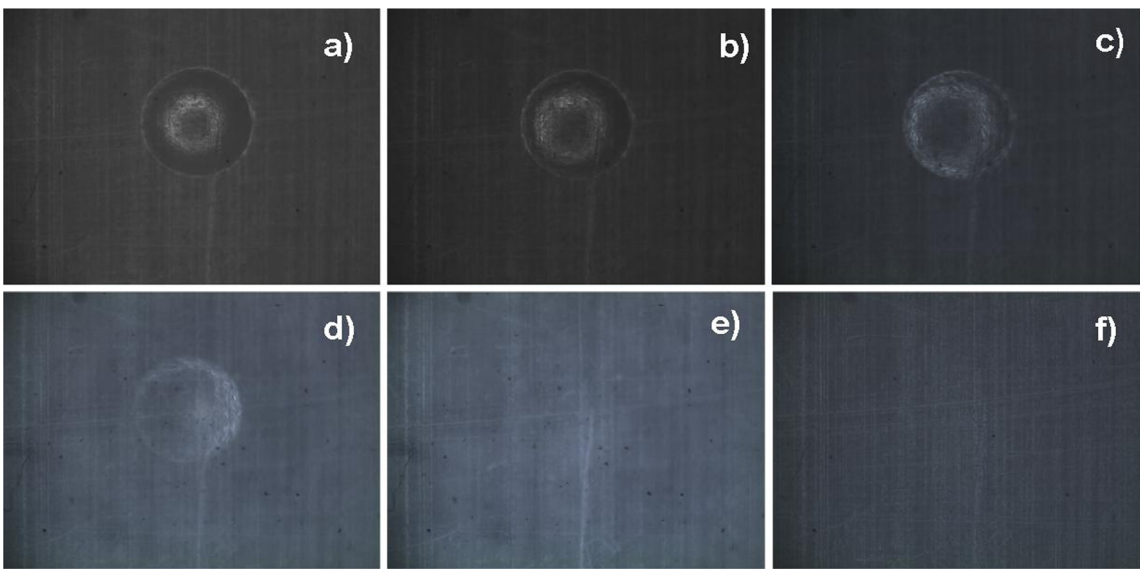

Fig. 6 Recovery process for 10 N hole in PCO-1 at: (**a**) 22.9ºC, (**b**) 36ºC, (**c**) 43ºC, (**d**) 46ºC, (**e**) 51ºC, (**f**) cooled (*recovered*)

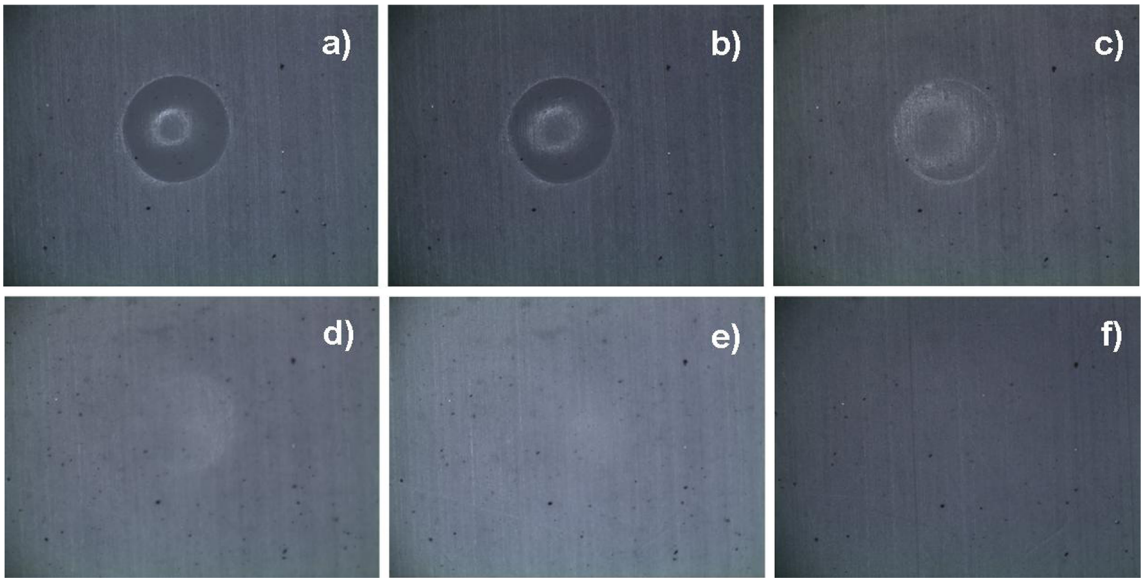

Fig. 7 Recovery process for 10 N hole in PCO-2 at: (**a**) 23.8ºC, (**b**) 32ºC, (**c**) 37ºC, (**d**) 41ºC, (**e**) 43ºC, (**f**) cooled (*recovered*)

amorphous phases leads to elastic recovery and relax back of a fraction of indentation strain, which is higher when DCP content increases and produces lower remaining hole depths (Fig. 5) [45–47]. Nevertheless, specific micro hardness analysis to evaluate cooperative effects of both phases under different crystallization conditions and indentation protocols should be performed to corroborate this performance, which is not object of this study.

On the other hand, the evolution of recovery process with temperature was monitored by optical microscopy. The sample was placed at room temperature on a heating surface and series of photos of the hole were taken when temperature was increasing. When recovery process was finished, the sample was slowly cooled to room temperature. Variations in the brightness in photos come from melting process of crystallites and turning the samples into transparent. Nevertheless, when cooled down they return to original translucent white colour. Figures 6, 7, 8 show the evolution of the hole marks with temperature for the PCO-1, PCO-2 and PCO-3 samples, respectively, assessing surface-repairing features from the shape memory properties of this kind of SMPs.

In parallel, the analysis of maximum depth of indentations with temperature for edgewise samples by optical microscopy allows evaluating shape recovery ratios, calculated by equation (1), as well as actuation temperatures profiles. Figure 9 shows as an example of recovery process for indented PCO-2

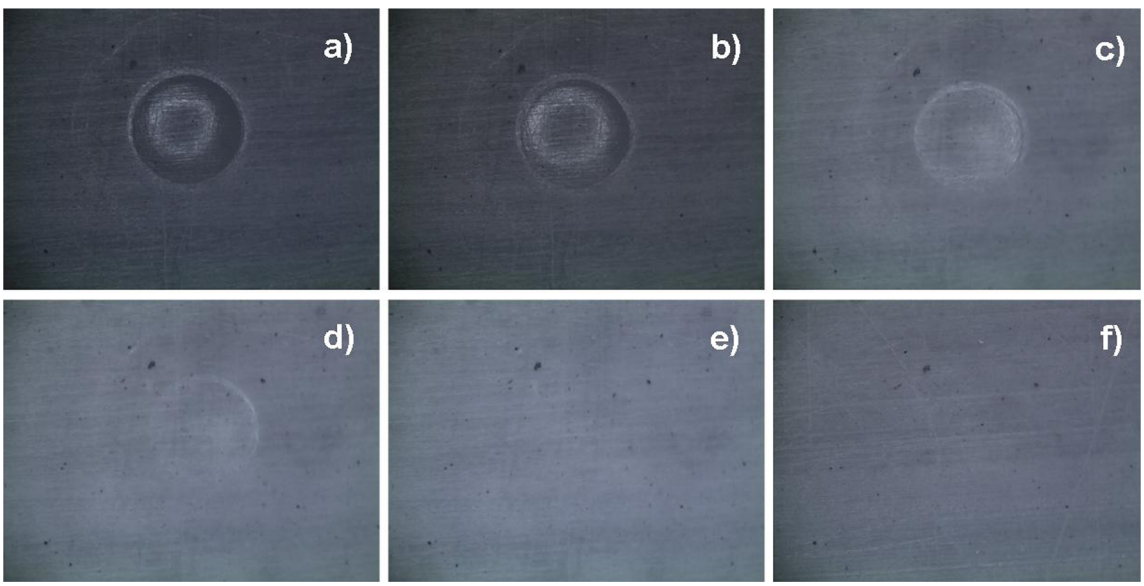

Fig. 8 Recovery process for 10 N hole in PCO-3 at: (**a**) 23.9ºC, (**b**) 29ºC, (**c**) 33ºC, (**d**) 35ºC, (**e**) 37ºC, (**f**) cooled (*recovered*)

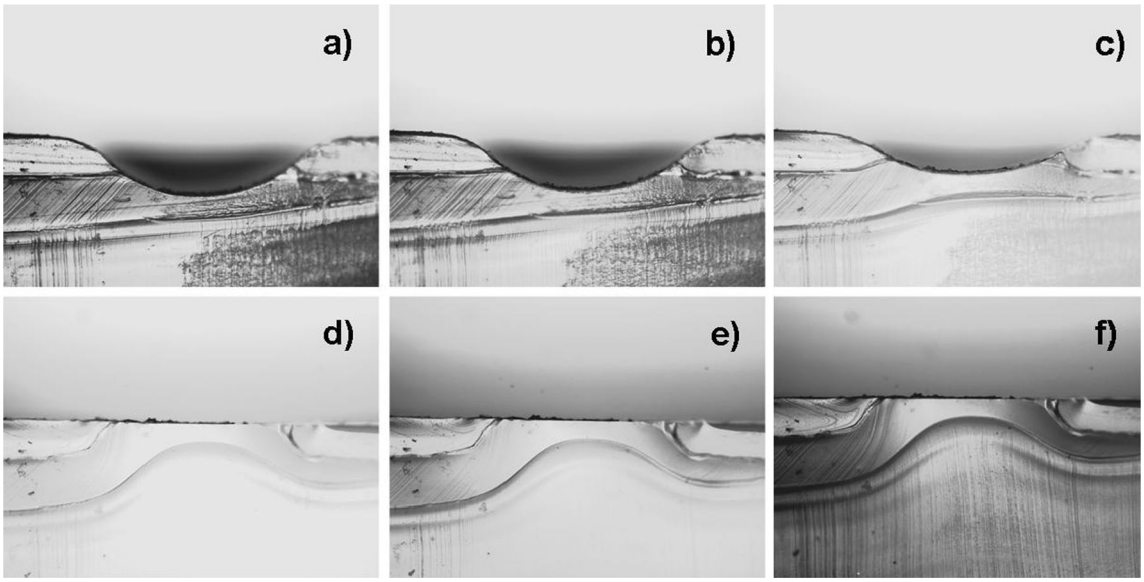

Fig. 9 Edgewise view of the recovery process for 10 N hole in PCO-2 at: (**a**) 24ºC, (**b**) 31ºC, (**c**) 36ºC, (**d**) 42ºC, (**e**) 44ºC, (**f**) cooled (*recovered*)

sample. Furthermore, the respective shape recoveries with temperature are represented in Fig. 10, where it can be observed the described shape recovery ratios of 100 %.

$$\text{recovery } \% = \frac{|D_T - D_0|}{D_0} \cdot 100 \begin{cases} D_0 = \text{initial depth} \\ D_T = \text{depth at each temperature} \end{cases} \quad (1)$$

Finally, self-repair of the scratch-marked samples was demonstrated by surface profilometry (both measuring techniques were demonstrated as suitable tools for evaluation and it are faster and easier to use than confocal microscopy).

Figures 11 and 12 show some of the profiles measured with the profilometry technique for the PCO-0 and PCO-2 samples, respectively, when they are line-marked. As can been observed in Fig. 11, the PCO-0 sample has no shape memory properties, as well as losses dimensional stability from null crosslinking preventing specimens from flowing like a viscous liquid. However, in Fig. 12 it can be seen that the sample with covalent bonds in polymer network is characterized by shape memory features and subsequent exhibited self-repairing properties.

In conclusion, when the PCO-DCP crosslinked samples were heated above its transition temperature the surface defects disappear (holes or lines/scratches), which demonstrates the potential self-repair response under temperature of these new polymeric materials, based on their shape memory behaviour, with functional or aesthetic applications.

Conclusions

Thermal-activated self-repair features of a series of crosslinked PCO samples were demonstrated by evaluating

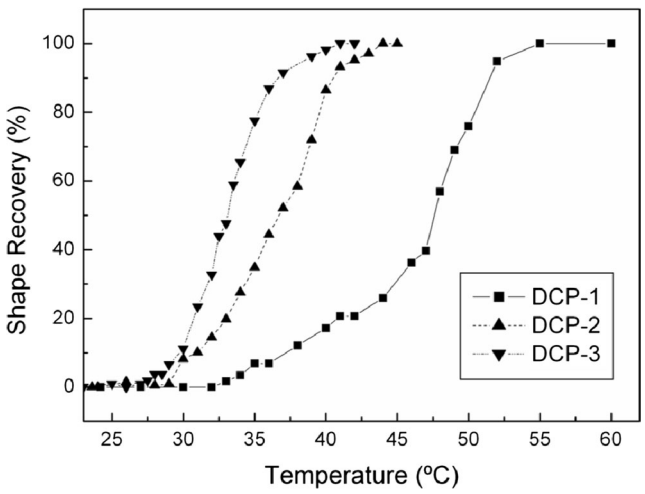

Fig. 10 Shape recovery with temperature

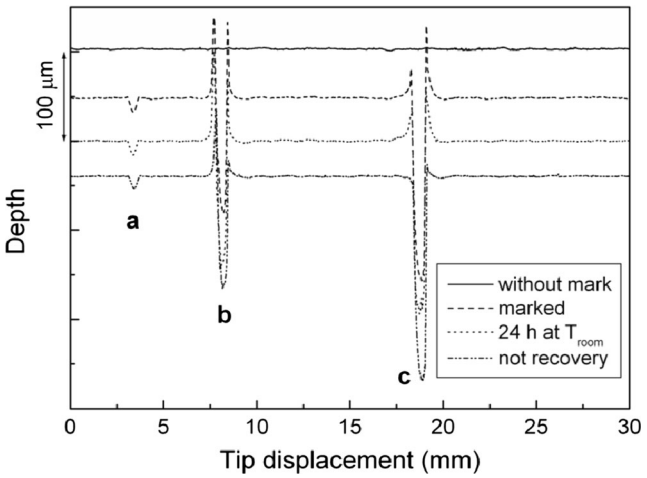

Fig. 11 Measured profiles for PCO-0 sample: (**a**) 5 N, (**b**) 10 N and (**c**) 15 N

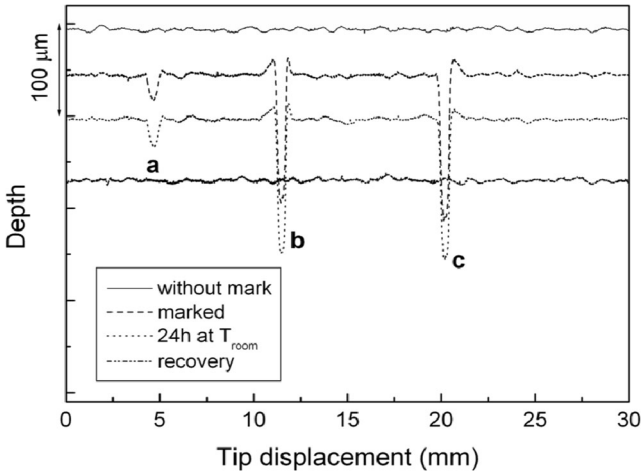

Fig. 12 Measured profiles for PCO-2 sample: (**a**) 5 N, (**b**) 10 N and (**c**) 15 N

the recovery of plastic deformations performed with different indentation and scratching forces. The correlation of the influence of crosslinking density on thermal properties of these shape memory semi-crystalline polymers with thermal-induced surface self-repairing was evaluated. Thus, different marking processes and recovery features were monitored by surface and optical-confocal profilometry, together with optical microscopy, to demonstrate potential applications of this smart performance in, for example, aesthetic or functional related purposes, apart from other temperature-sensing elements.

Acknowledgments The authors would like to acknowledge Basque Country Government (ACTIMAT project from ETORTEK programme) for the financial support.

References

1. Schmets AJM, van der Zaken G, van der Zwaag S (2007) Self healing materials: an alternative approach to 20 centuries of materials science. Springer, Dordrecht
2. Wu DY, Meure S, Solomon D (2008) Self-healing polymeric materials: A review of recent developments. Prog Polym Sci 33:479–522. doi: http://dx.doi.org/10.1016/j.progpolymsci.2008.02.001
3. White SR, Sottos NR, Geubelle PH et al (2001) Autonomic healing of polymer composites. Nature 409:794–797. doi:10.1038/35057232
4. Rule JD, Brown EN, Sottos NR et al (2005) Wax-protected catalyst microspheres for efficient self-healing materials. Adv Mater 17:205–208. doi:10.1002/adma.200400607
5. Cho SH, Andersson HM, White SR et al (2006) Polydimethylsiloxane-based self-healing materials. Adv Mater 18:997–1000. doi:10.1002/adma.200501814
6. Gupta S, Zhang Q, Emrick T et al (2006) Entropy-driven segregation of nanoparticles to cracks in multilayered composite polymer structures. Nat Mater 5:229–233. doi:10.1038/nmat1582
7. Kolmakov GV, Matyjaszewski K, Balazs AC (2009) Harnessing labile bonds between nanogel particles to create self-healing materials. ACS Nano 3:885–892. doi:10.1021/nn900052h
8. Toohey KS, Sottos NR, Lewis JA, et al. (2007) Self-healing materials with microvascular networks. Nat Mater 6:581–585. doi:http://www.nature.com/nmat/journal/v6/n8/suppinfo/nmat1934_S1.html
9. Toohey KS, Hansen CJ, Lewis JA et al (2009) Delivery of Two-part self-healing chemistry via microvascular networks. Adv Funct Mater 19:1399–1405. doi:10.1002/adfm.200801824
10. Hansen CJ, Wu W, Toohey KS et al (2009) Self-healing materials with interpenetrating microvascular networks. Adv Mater 21:4143–4147. doi:10.1002/adma.200900588
11. South AB, Lyon LA (2010) Autonomic self-healing of hydrogel thin films. Angew Chemie 122:779–783. doi:10.1002/ange.200906040
12. Mukhopadhyay P, Fujita N, Takada A et al (2010) Regulation of a real-time self-healing process in organogel tissues by molecular adhesives. Angew Chemie Int Ed 49:6338–6342. doi:10.1002/anie.201001382
13. Amamoto Y, Kamada J, Otsuka H et al (2011) Repeatable photoinduced self-healing of covalently cross-linked polymers through reshuffling of trithiocarbonate units. Angew Chemie 123:1698–1701. doi:10.1002/ange.201003888
14. He L, Fullenkamp DE, Rivera JG, Messersmith PB (2011) pH responsive self-healing hydrogels formed by boronate – catechol complexation. Chem Commun 47:7497–7499. doi:10.1039/c1cc11928a
15. Lai S-M, Lan Y-C (2013) Shape memory properties of melt-blended polylactic acid (PLA)/thermoplastic polyurethane (TPU) bio-based blends. J Polym Res 20:1–8. doi:10.1007/s10965-013-0140-6
16. Schmidt C, Sarwaruddin Chowdhury AM, Neuking K, Eggeler G (2011) Thermo-mechanical behaviour of shape memory polymers, e.g., tecoflex® by 1WE method: SEM and IR analysis. J Polym Res 18:1807–1812. doi:10.1007/s10965-011-9587-5
17. Revathi A, Rao S, Rao KV (2013) Effect of strain on the thermomechanical behavior of epoxy based shape memory polymers. J Polym Res 20:113. doi:10.1007/s10965-013-0113-9
18. Biju R, Nair CPR (2013) Synthesis and characterization of shape memory epoxy-anhydride system. J Polym Res 20:1–11. doi:10.1007/s10965-013-0082-z
19. Kavitha, Revathi A, Rao S et al (2012) Characterization of shape memory behaviour of CTBN-epoxy resin system. J Polym Res 19:1–7. doi:10.1007/s10965-012-9894-5
20. Lendlein A, Kelch S (2002) Shape-memory polymers. Angew Chemie Int Ed 41:2034–2057. doi:10.1002/1521-3773(20020617)41:12<2034::aid-anie2034>3.0.co;2-m
21. Liu C, Qin H, Mather PT (2007) Review of progress in shape-memory polymers. J Mater Chem 17:1543–1558. doi:10.1039/b615954k
22. Amirian M, Nabipour Chakoli A, Sui J, Cai W (2012) Enhanced shape memory effect of poly(L-lactide-co-ε-caprolactone) biodegradable copolymer reinforced with functionalized MWCNTs. J Polym Res 19:1–10. doi:10.1007/s10965-011-9777-1
23. El Feninat F, Laroche G, Fiset M, Mantovani D (2002) Shape memory materials for biomedical applications. Adv Eng Mater 4:91–104. doi:10.1002/1527-2648(200203)4:3<91::AID-ADEM91>3.0.CO;2-B
24. Wang Y, Zhu G, Tang Y et al (2014) Mechanical and shape memory behavior of chemically cross-linked SBS/LDPE blends. J Polym Res 21:1–10. doi:10.1007/s10965-014-0405-8
25. Alonso-Villanueva J, Cuevas JM, Laza JM et al (2010) Synthesis of poly(cyclooctene) by ring-opening metathesis polymerization: characterization and shape memory properties. J Appl Polym Sci 115:2440–2447. doi:10.1002/app.29394
26. Xie T (2011) Recent advances in polymer shape memory. Polymer 52:4985–5000. doi: http://dx.doi.org/10.1016/j.polymer.2011.08.003
27. Rodriguez ED, Luo X, Mather PT (2011) Linear/network poly(ε-caprolactone) blends exhibiting shape memory assisted self-healing (SMASH). ACS Appl Mater Interfaces 3:152–161. doi:10.1021/am101012c

28. Wang W, Jin Y, Ping P et al (2010) Structure evolution in segmented poly(ester urethane) in shape-memory process. Macromolecules 43: 2942–2947. doi:10.1021/ma902781e
29. Ping P, Wang W, Chen X, Jing X (2005) Poly(ε-caprolactone) polyurethane and its shape-memory property. Biomacromolecules 6:587–592. doi:10.1021/bm049477j
30. Xiao X, Xie T, Cheng Y-T (2010) Self-healable graphene polymer composites. J Mater Chem 20:3508–3514. doi:10.1039/c0jm00307g
31. Li G, Nettles D (2010) Thermomechanical characterization of a shape memory polymer based self-repairing syntactic foam. Polymer 51: 755–762. doi:10.1016/j.polymer.2009.12.002
32. Cuevas JM, Laza JM, Rubio R et al (2011) Development and characterization of semi-crystalline polyalkenamer based shape memory polymers. Smart Mater Struct 20:035003/1–035003/9. doi:10.1088/0964-1726/20/3/035003
33. Khonakdar HA, Jafari SH, Rasouli S et al (2007) Investigation and modeling of temperature dependence recovery behavior of shape-memory crosslinked polyethylene. Macromol Theory Simul 16:43–52. doi:10.1002/mats.200600041
34. Rezanejad S, Kokabi M (2007) Shape memory and mechanical properties of cross-linked polyethylene/clay nanocomposites. Eur Polym J 43:2856–2865. doi: http://dx.doi.org/10.1016/j.eurpolymj.2007.04.031
35. Li F, Zhu W, Zhang X et al (1999) Shape memory effect of ethylene–vinyl acetate copolymers. J Appl Polym Sci 71:1063–1070. doi:10.1002/(sici)1097-4628(19990214)71:7<1063::aid-app4>3.0.co;2-a
36. Liu C, Chun SB, Mather PT et al (2002) Chemically cross-linked polycyclooctene: synthesis, characterization, and shape memory behavior. Macromolecules 35:9868–9874. doi:10.1021/ma021141j
37. Liu C, Mather PT (2002) Thermomechanical characterization of a tailored series of shape memory polymers. J Appl Med Polym 6:47–52
38. Mather PT, Liu C, Chun SB, Coughlin EB (2007) Patent US7173096 B2
39. Lendlein A (2007) Pat. WO 2007/060022 A1
40. Cuevas JM, Rubio R, Laza JM et al (2012) Shape memory composites based on glass-fibre-reinforced poly(ethylene)-like polymers. Smart Mater Struct 21:035004/1–035004/9. doi:10.1088/0964-1726/21/3/035004
41. Cuevas JM, Alonso J, German L, et al. (2009) Magneto-active shape memory composites by incorporating ferromagnetic microparticles in a thermo-responsive polyalkenamer. Smart Mater Struct 18:075003/1–075003/10. doi: 10.1088/0964-1726/18/7/075003
42. Cuevas JM, Rubio R, German L et al (2012) Triple-shape memory effect of covalently crosslinked polyalkenamer based semicrystalline polymer blends. Soft Matter 8:4928–4935. doi:10.1039/c2sm07481h
43. Céspedes RIN, Gámez JFH, Velázquez MGN et al (2014) Thermoplastic elastomers based on high-density polyethylene, ethylene–propylene–diene terpolymer, and ground tire rubber dynamically vulcanized with dicumyl peroxide. J Appl Polym Sci 131: 39901/1–39901/8. doi:10.1002/app.39901
44. Nakayama K, Watanabe T, Ohtake Y, Furukawa M (2008) Influence of residual peroxide on the degradation of peroxide-crosslinked ethylene–propylene–diene rubber. J Appl Polym Sci 108:2578–2586. doi:10.1002/app.27894
45. Baltá-Calleja EJ, Kilian HG (1985) A novel concept in describing elastic and plastic properties of semicrystalline polymers: polyethylene. Colloid Polym Sci 263:697–707. doi:10.1007/BF01422850
46. Deslandes Y, Rosa EA, Brisse F, Meneghini T (1991) Correlation of micro hardness and morphology of poly (ether-ether-ketone) films. J Mater Sci 26:2769–2777. doi:10.1007/BF00545567
47. Calleja FJB, Salazar JM, Čačković H, Loboda-Čačković J (1981) Correlation of hardness and microstructure in unoriented lamellar polyethylene. J Mater Sci 16:739–751. doi:10.1007/BF02402791